Charge distributions and oxidation states in Mn-based oxidants from *ab initio* molecular dynamics simulation

Colin Crago¹, Shifa Zhong², Siddharth Rajupet¹, Huichun Zhang², Daniel J. Lacks¹ Department of Chemical and Biomolecular Engineering ²Department of Civil and Environmental Engineering Case Western Reserve University Cleveland, OH 44106

Abstract

Organic contaminants can be removed from water/wastewater by oxidative degradation, using oxidants such as manganese oxides and/or aqueous manganese ions. The Mn species show a wide range of activity, which is related to the oxidation state of Mn. Here, we use ab initio molecular dynamics simulations to address Mn oxidation states in these systems. We first develop a correlation between Mn partial atomic charge and the oxidation state, based on results of 31 simulations on known Mn aqueous complexes. The results collapse to a master curve; the dependence of partial atomic charge on oxidation state weakens with increasing oxidation state, which concurs with a previously proposed feedback effect. This correlation is then used to address oxidation states in Mn systems used as oxidants. Simulations of MnO₂ polymorphs immersed in water give average oxidation states (AOS) in excellent agreement with experimental results, in that β -MnO₂ has the highest AOS, α -MnO₂ has an intermediate AOS, and δ -MnO₂ has the lowest AOS. Furthermore, the oxidation state varies substantially with the atom's environment, and these structures include Mn(III) and Mn(V) species that are expected to be active. In regard to the MnO₄-/HSO₃-/O₂ system that has been shown to be a highly effective oxidant, we propose a novel Mn complex that could give rise to the oxidative activity, where Mn(III) is stabilized by sulfite and dissolved O₂ ligands. Our simulations also show that the O₂ would be activated to O₂²⁻ in this complex under acidic conditions, and could lead to the formation of OH radicals that serve as oxidants.

1. Introduction

Ecosystems and human health are threatened by anthropogenic organic compounds in surface and ground water, which often enter the environment through wastewater discharge. ¹ For example, hormonal responses of animals and humans are altered by endocrine disruptors such as bisphenol A, a heavily-used precursor in polycarbonate production. ^{2,3} Antibacterial-resistant strains of pathogens are promoted by chemicals used for different purposes, including antibacterial additives, such as triclosan, and personal care products.⁴

Organic contaminants can be removed from wastewater by oxidative degradation. Amorphous and crystalline manganese oxides 5,6,7 and aqueous manganese ions, 8,9,10,11,12,13 are promising oxidants for this purpose. These oxidants, however, show a wide range of activity, the reasons for this variation are not well understood. The predominant line of thought is that the oxidative activity is related to the oxidation state of Mn. Mn with an oxidation state of three, Mn(III), is thought to act as a particularly effective oxidant, and the oxidative activity of manganese oxides has been examined in terms of Mn(III) content. Some studies found that crystal polymorphs with a stoichiometry that generates Mn(III) species have higher oxidative activity, 14 but other studies found that this conclusion does not hold generally for all reactions. 15 In regard to the wastewater-relevant reaction of bisphenol A, the oxidative activity was found to vary significantly between MnO₂ crystalline polymorphs, in a way that correlated with spectroscopic signatures of Mn(III) content. 16 To further complicate the situation, evidence suggests that surface defects may play an important role in oxidative activity. 17,18,19

Mn(III) is also thought to be important in aqueous solutions. Organic contaminants can be degraded in reactions oxidized by MnO₄^{-,20} where the oxidation state is Mn(VII). However, the reaction rate is several orders of magnitude faster when HSO₃⁻ is added, presumably due to the formation of Mn(III) from the reaction of MnO₄⁻ and HSO₃⁻.¹¹⁻¹³ While Mn(III) is not stable as an isolated ion in aqueous solutions, it can be stabilized by ligands. In some cases, ligands are attached intentionally to stabilize Mn(III),²¹ while in other cases the complexation occurs naturally with (often-unknown) ligands.²² Our recent study demonstrated that the enhanced catalytic activity in MnO₄⁻/HSO₃⁻ is furthermore dependent on dissolved oxygen in the solution, ²³ presumably because Mn(III) is stabilized by both HSO₃⁻ and dissolved O₂. However, the identity of the complex that stabilizes Mn(III), and how oxygen participates in the catalytic process, are open questions. Moreover, other Mn oxidation states, such as Mn(V) and Mn(VI), may play important roles in oxidation as well. For example, MnO₄⁻/HSO₃⁻ rapidly oxidizes methyl phenyl sulfoxide while MnO₂/HSO₃⁻ does not, which led to the suggestion that Mn(V) is the active species.^{24,25}

Despite the utility of oxidation states, their relationship to fundamental molecular-level properties is not clear. Oxidation states are obtained from a set of simple rules that conceptually shift electrons between atoms so that each atom has an empty or full valence electron octet. ^{26,27} For example, in KMnO₄, all atoms have empty or full octets when the atoms have the formal charges K⁺¹, Mn⁺⁷, and O⁻²; thus Mn is said to have the oxidation state Mn(VII). On the other hand, rigorous quantum chemistry gives a continuous electron density distribution throughout the system. The electron distribution can be partitioned to atoms by various algorithms, to give partial atomic charges. At first glance, it might seem that the partial atomic charges would equal the oxidation state—but this is not the case. ^{28,29,30,31,32,33,34} One reason for this discrepancy is that the idea of partitioning electrons to atoms is fundamentally flawed, due to the delocalized nature of the electrons and the arbitrariness of any partitioning scheme. But more significantly, a feedback effect occurs for the electron distributions—as more electrons are transferred to a given atom, the

electron-electron repulsion causes this electron distribution to be increasingly spread out away from the atom center. The feedback effect therefore leads to a weakened dependence of partial atomic charge on the oxidation state.³⁵

While there is no rigorous relationship between oxidation state and partial atomic charge, some studies have shown that these quantities do appear to be correlated in metal oxide systems, the class of systems that we are interested in. A correlation has been shown over two or three systems with different oxidation states: Mn(H₂O)_x complexes;³⁶ MnO and MnO₂;³⁷ Pd₂O, PdO and PdO₂;³⁸ and Cu₂O and CuO.³⁹ However, we are not aware of studies that addressed whether a correlation would hold over a more extensive set of systems.

Here, we examine oxidation states in manganese systems that serve as oxidants for water/wastewater treatment, using *ab initio* molecular dynamics simulations. We first construct a correlation between partial atomic charge and oxidation state for Mn systems, based on an extensive set of 31 simulations of known Mn ion complexes in aqueous solution. We then address oxidation states in three MnO₂ polymorphs immersed in water. In contrast to ideal crystal surfaces, our simulations on nanoscale structures feature a variety of Mn environments and types of interactions with water, which could yield insights into the behavior of surface defects. We also propose aqueous Mn complexes that could give the MnO₄-/HSO₃-/O₂ system the catalytic activity that we showed experimentally,²³ and we analyze the stability and oxidation states of these complexes.

2. Computational methods

Ab initio molecular dynamics simulations were carried out using density functional theory (DFT) implemented in the SIESTA software package.⁴⁰ These simulations are based on the Born-Oppenheimer approximation, in which the electron distribution, energy and forces between nuclei are found at each time step by solving the DFT approximation of the Schrödinger equation.⁴¹ The trajectory of the nuclei is obtained by numerically integrating the classical equations of motion with these forces.

Simulations for aqueous manganese ion complexes were carried out with 40 to 70 water molecules, and 0 to 7 counter ions. These systems are made up of \sim 120-250 atoms. Periodic boundary conditions were used in order to model behavior in a bulk water phase. The simulations were carried out in the NVT ensemble with cell dimensions chosen to achieve an overall density of 1 g/L; the simulation cells had edge-lengths ranging from 11.0 to 13.7 Å.

Simulations were carried out on nanoscale structures of α -MnO₂, β -MnO₂, and δ -MnO₂ polymorphs composed of 16, 10 and 9 MnO₂ units, respectively. These simulations also included 120, 80 and 53 water molecules, respectively. Again, periodic boundary conditions were used in order to model behavior in a bulk water phase. The simulations were carried out in the NPT ensemble at atmospheric pressure; the simulation cells had edge-lengths ranging from 11.6 to 14.9 Å.

The *ab initio* molecular dynamics simulations are extremely computationally intensive, and only allow simulations on the order of picoseconds. This timescale is too short to ensure the equilibration of the water molecules, in regard to the formation of the hydrogen bonded network of water molecules in the water phase, as well as the proper orientation of water molecules near the complex. Therefore, as a first step in preparing the simulation cell, we used a force-field-based

molecular dynamics simulation to equilibrate the system. This simulation was run for about 5 ns, using the GROMACS software package. ⁴² The final configuration of the force-field-based simulation was used as the starting configuration for the *ab initio* molecular dynamics simulation.

The *ab initio* electron structure calculations were carried out with the PBE generalized gradient approximation for the exchange-correlation functional.⁴³ Double zeta basis sets with polarization and norm-conserving Troullier-Martins pseudopotentials⁴⁴ were used. The energy convergence threshold used for the self-consistent field cycle was 10⁻⁴ eV. The trajectories of the nuclei were numerically integrated with a time step of 1 fs. Temperature was controlled with a Nosé thermostat at 300 K, and pressure in the MnO₂ polymorph simulations is controlled with the Parrinello-Rahman method at 1 atmosphere. The simulations were carried out for durations of 1 - 5 ps.

Partial atomic charges were determined using the Bader method,⁴⁵ in which each atom is assigned the electron distribution within the region defined by positions of minima in the charge density separating this atom's nucleus from its neighboring atoms' nuclei. The Bader charge calculation is carried out using the code from Henkelman *et. al.*^{46,47} Partial atomic charges were determined at five equally spaced time intervals during the final 20% of the simulation, and the average of these values was used.

3. Results and Discussion

Our strategy was to first develop a correlation between the partial atomic charge and the oxidation state of Mn ions, based on results for simulations with a series of known Mn complexes. We then used this correlation to determine Mn oxidation states in MnO₂ polymorphs, and in novel Mn complexes that we propose to possibly give rise to oxidative activity in the MnO₄ $^-/HSO_3^-/O_2$ system.

3.1. Correlating Mn partial atomic charge with oxidation state

A series of simulations was carried out on aqueous solutions involving five Mn ion complexes, which are shown in Fig. 1. These complexes were selected because they are well known and cover a wide range of oxidation states in their most favorable forms; for instance, KMnO₄ has an Mn oxidation state of +7, the isolated Mn ion typically has an oxidation state of +2, and the other complexes have oxidation states that lie between these values. To generate more data points with different Mn oxidation states, various numbers of K and Cl atoms were systematically added as additional solutes, with the expectation that they would ionize—as the overall system is neutral, changing the number of ions in the system changes the formal charge of the Mn complex, and therefore the oxidation state of the Mn ion. The systems that were simulated is listed in Table 1.

Ab initio molecular dynamics simulations were carried out for each system for 1 ps. System properties, such as potential energy, were monitored to confirm that the system equilibrated. The partial atomic charge for each atom was then obtained from the Bader method.

In all cases, the partial charge of K atom i, $Q_{K,i}$, was +1.00. Thus the K atoms always fully ionized with formal charge $Z_K = +1$. In contrast, the partial atomic charge of Cl atom i, $Q_{Cl,i}$, varied between nearly zero and a maximum magnitude $Q_{Cl,max} = -0.64$. We therefore considered Cl atoms

with charge $Q_{Cl,max}$ to be fully ionized, and Cl atoms with a smaller charge to be partially ionized. In general, the formal charge of Cl atom i, $Z_{Cl,i}$, was obtained as

$$Z_{Cl,i} = -\frac{Q_{Cl,i}}{Q_{Cl,max}} \tag{1}$$

Most chlorine atoms had charge $Q_{Cl,i}$ near $Q_{Cl,max}$, and were fully ionized.

Chemical reactions occurred in some of the simulations, which changed the number or types of ions in the system. In some cases, two Cl⁻ ions combined,

$$2Cl^- \to Cl_2 + 2e^- \tag{2}$$

In other cases, a Cl⁻ ion reacted with an H₂O molecule,

$$C1^- + H_2O \rightarrow HC1O + H_3O^+ + 2e^-$$
 (3)

The sum of the partial atomic charges on an H_3O^+ ion was always close to +0.4. To relate this value to the formal charge, we note that in water the partial atomic charges of the O and H atoms are -0.8 and 0.4, respectively. Since the O and H atoms in water have formal charges of -2 and +1, respectively, we conclude that the hydronium charge of 0.4 corresponds to the formal charge $Z_{H_3O} = +1$.

The formal charge of the Mn complex, Z_{Mn-X} , was obtained as that which balances the sum of the formal charges of the ions in the system,

$$Z_{Mn-X} = \sum_{i}^{n_{Cl}} Z_{Cl,i} - n_K Z_K - n_{H_3O} Z_{H_3O}$$
 (4)

where n_K and n_{H_30} are the numbers of potassium and hydronium ions in solution, respectively. Note that the charge on the water molecules in the system was found to be negligible.

The formal charge on the Mn atom, Z_{Mn} , was then determined by accounting for the formal charges of the remainder of the complex, Z_X ,

$$Z_{Mn} = Z_{Mn-X} - Z_X \tag{5}$$

The values of Z_X for the various complexes are given in Table 1. The oxidation state of Mn is equal to Z_{Mn} .

The Mn oxidation states and partial atomic charges for these simulations are given in Table 1. Note that the ions in solution sometimes differ from the atoms added to the system due to chemical reactions (Eqs. 2 and 3), and the formal charge of the Mn complex is sometimes non-integer due to partial ionization of chlorine atoms (see Eqs. 1 and 4).

The partial atomic charges of Mn are plotted as a function of oxidation state in Fig. 2. The results for all 32 systems collapse to a single master curve. The dependence of partial atomic charge on oxidation state is nonlinear, and the increase in charge with increasing oxidation state weakens as the oxidation state increases. This result concurs with the feedback mechanism described previously³⁵—as more electrons are transferred to an atom, the electron distribution increasingly spreads out due to electron-electron repulsion, leading to a weakened dependence of partial atomic charge on oxidation state. The results in Fig. 2 were fit to the three-parameter function, $Q_{Mn} = A - Be^{-CZ_{Mn}}$, where $A = 1.891 \pm 0.025$, $B = 2.10 \pm 0.35$, and $C = 0.70 \pm 0.10$. This equation is inverted to give the Mn oxidation state as a function of partial atomic charge,

$$Z_{Mn} = -\frac{1}{c} ln \left(\frac{A - Q_{Mn}}{B} \right) \tag{6}$$

Eq. 6 was used to estimate Mn oxidation states in other systems, using simulation results for the Mn partial atomic charge.

3.2. Estimation of Mn oxidation states in MnO₂ polymorphs

We investigate oxidation states of Mn at surfaces of α -MnO₂, β -MnO₂, and δ -MnO₂. These polymorphs are all based on [MnO₆] octahedral units, but the different topologies of these units in the polymorphs gives rise to different structural motifs: α -MnO₂ features broad tunnels, β -MnO₂ is close packed, and δ -MnO₂ is composed of weakly-bound layers. Wulff construction analyses using DFT calculations determined the equilibrium crystal morphology of α - and β -MnO₂ and identified the crystallographic planes that define the equilibrium morphology; ^{18,48} for δ -MnO₂, the equilibrium morphology consists of single-atom-thick layers that loosely bound. The stable surfaces have Mn ions with coordination numbers ranging from 3 to 6 for α -MnO₂, and ranging from 4 to 6 for β -MnO₂.

Real surfaces, however, are imperfect rather than ideal crystallographic planes, and have defects including step edges, oxygen vacancies, local disorder, etc.; these defects are likely to play important roles in the oxidative activity of MnO₂. ^{17,18,19} Furthermore, we are interested in the properties of MnO₂ in water environments, and water interacts significantly with oxide surfaces through both non-dissociative and dissociative modes. ^{49,50,51} These two considerations are likely coupled, as the interactions with water can stabilize the defects.

Here, we address imperfect surfaces that interact with water by simulating nanoscale structures of MnO_2 polymorphs immersed in water. The nanoscale α - MnO_2 , β - MnO_2 , and δ - MnO_2 structures we simulate, shown in Fig. 3, contain 16, 10 and 9 MnO_2 units, respectively. These structures have Mn coordination numbers ranging from 2 to 6, and thus display a broad range of Mn environments. This approach differs from previous studies of MnO_2 surfaces that we are aware of, which model semi-infinite slabs of MnO_2 that expose particular crystallographic planes as the slab surfaces; each approach has advantages, with an advantage of the present approach being that the environments of the atoms in these structures may act as models of defect sites in crystals.

Ab initio molecular dynamics simulations were carried out for the α -MnO₂, β -MnO₂, and δ -MnO₂ structures in water for 1 ps. We monitored the potential energy and volume to confirm that the system has equilibrated, and then determined properties of the system. The structure was characterized in regard to the interactions with water. The partial atomic charge for each atom was obtained from the Bader method.

The interactions of the under-coordinated Mn atoms with water were significant, and included both non-dissociative and dissociative interactions. In some cases, an H₂O molecule bonded to an Mn atom via its O atom, and the H₂O molecule became fixed in place as part of the crystal structure. In other cases, an H₂O molecule dissociated to OH⁻ and H⁺—the OH⁻ group bonded to an Mn atom, and the residual H⁺ bonded to a crystalline O atom (which converted the crystalline O atom into an OH⁻ group). These water interactions increased the coordination number of under-coordinated Mn atoms, such that almost every Mn atom had six O atom neighbors of some form (in the form of O, OH or H₂O). Fig. 4 shows snapshots from the simulation of β-MnO₂ which highlight the interactions with water at two Mn sites; this figure shows that these Mn atoms have octahedral coordination when interactions with water are included, and that both non-dissociative and dissociative interactions occur. For the α, β, and δ-MnO₂ polymorphs, 100%, 80%

and 89% of the Mn atoms, respectively, had coordination numbers of six when the interactions with strongly bound H₂O or OH are included. Previous studies on β-MnO₂ crystallographic surfaces also showed that the water interactions acted to complete the octahedral coordination of under-coordinated surface Mn atoms.⁴⁹

The extent of H_2O dissociation varied with the polymorph. In δ -MnO₂, only one Mn atom was bonded to an OH group; in α -MnO₂, two-thirds of the Mn atoms were bonded to an OH group; and in β -MnO₂, all of the Mn atoms were bonded to an OH group, with most of the Mn atoms being bonded to two or more OH groups. Previous work showed that the propensity of water to dissociate at oxide surfaces depended on both the oxide composition and the particular crystallographic surface, and that the dissociation is driven by under-coordinated surface O atoms appropriating an H^+ from the H_2O to in order to complete the three-fold coordination. Our results for the variation of H_2O dissociation between polymorphs can be understood in this light. The increased H_2O dissociation from δ -MnO₂ to α -MnO₂ to β -MnO₂ follows the increased fraction of under-coordinated O atoms in the structures that we simulated—55% under-coordinated O atoms in the δ -MnO₂ structure, 63% in the α -MnO₂ structure, and 80% in the β -MnO₂ structure (note that these percentages are for the nanoscale structures we simulated, and not for crystallographic surfaces of these polymorphs).

The results for the partial atomic charges for the Mn atoms in the MnO_2 polymorphs are shown in Table 2. The Mn oxidation states were determined using the correlation in Eq. 6, and are also shown in Table 2. In general, the atoms in positions that are equivalent by symmetry have similar values, as indicated by the small uncertainty values in Table 2, which suggests that the results are well equilibrated (there is one exception, where there is a large uncertainty for one of the positions in δ -MnO₂; here, we believe that the water molecules have not fully equilibrated around one of the Mn atoms).

The broad range of Mn oxidation states in the MnO₂ structures, from 2.9 to 5.4, comes from the range of environments surrounding the Mn atoms. Fig. 4 highlights the local environments of two Mn atoms. These environments differ: although both Mn atoms have octahedral coordination, four of the six O neighbors have the full complement of 3 bonds for the Mn atom in frame a, but only two of the six O neighbors have this full complement in frame b. These different environments lead to different oxidation states—3.7 for the Mn atom in frame a, and 5.4 for the Mn atom in frame b.

In our previous work, we experimentally estimated the average oxidation state (AOS) in α , β , and δ -MnO₂ using two independent methods—analysis of the splitting of the Mn 3s XPS peak and chemical titration. ¹⁶ In Fig. 5, we compare our simulation results for the AOS with the experimental estimates. The simulation results for the AOS are close to the experimental results, but are consistently higher; since oxidation states do not rigorously connect to physical properties (as discussed in the Introduction), different routes to try to determine the oxidation state are expected to give somewhat different results. However, we see excellent agreement between our *ab initio* simulations and experiment for the trends in the AOS with polymorph, in that β -MnO₂ has the highest AOS, α -MnO₂ has an intermediate AOS, and δ -MnO₂ has the lowest AOS.

Our simulation results provide insight into two issues that have been discussed in regard to oxidation by MnO_2 . First, the simulations corroborate the systematic difference in the AOS of α , β , and δ -MnO₂ found experimentally; these differences in AOS correlate well with oxidation effectiveness, ¹⁶ and thus support the idea that Mn(III) is the active site for oxidation in these

systems. Second, since defects alter local environments for the Mn atoms, and local environments in turn alter Mn oxidation states, we expect defects in MnO₂ surfaces generate different oxidation states occurring near the defect sites, including Mn(III) and Mn(V) which are expected to be active.

3.3. Analysis of proposed $MnO_4^-/HSO_3^-/O_2$ catalyst systems

As discussed in the Introduction, the oxidative degradation of organic contaminants by MnO_4^- becomes orders of magnitude faster when HSO_3^- is added. Our previous experiments showed that this enhanced oxidative reactivity was furthermore dependent on dissolved oxygen in the solution, so that the active reactant is the system $MnO_4^-/HSO_3^-/O_2$. It has been suggested that the oxidative activity is due to Mn(III) $^{11-13}$, 23 or $Mn(V)^{24,25}$ species, where these oxidation states are stabilized by some unknown complex(es).

Here we examine thirteen complexes, shown in Fig. 6, that might act in the MnO₄⁻/HSO₃⁻/O₂ catalytic system. Complexes A-E are expected to have the oxidation state Mn(III), and complexes F-M are expected to have the oxidation state Mn(V). In some of the complexes the ligand is SO₃²⁻ rather than HSO₃⁻, because we anticipate that H⁺ may dissociate and dissolve into the water (this dissociation is in fact seen in the simulations).

Ab initio molecular dynamics simulations were carried out for each complex for 1 ps, and we examined whether the complex remained intact throughout the simulation. Simulations were carried out for the complex in pure water, with added K⁺ or Cl⁻ ions, and with added H₃O⁺ or OH ⁻ ions (to model behavior at different values of pH). Due to the small simulation size, one H₃O⁺ corresponds to pH near 0, while one OH⁻corresponds to a pH near 14.

Complex B was the only one of the proposed complexes that remained intact throughout the simulation. To further probe its stability, we ran a longer simulation (5 ps), and it remained intact throughout the longer simulation as well. Complex B remained stable in systems with no other ions, and in a system with one positive ion (either K⁺ or H₃O⁺). However, it was unstable with more than one positive ion in the system; in this case the O₂ group (O=O) on the complex split apart. Complex B was also unstable with negative ions in the system, in which case OH⁻ or O²⁻ (from dissociated water) ions became coordinated to the complex. Thus, we find that complex B is stable in neutral or acidic environments. This result concurs with experimental results that show that the system becomes less reactive at higher pH.¹¹

Complex E, which is similar to Complex B but with HSO_3^- as a ligand instead of $SO_3^{2^-}$, was found to transform to Complex B in simulations with one negative ion or no ions in solution, by donating its H^+ to the solution. With this H^+ added to the solution, the initially basic and neutral conditions became neutral and acidic conditions, respectively, and thus match the conditions that we found led to stable Complex B. Complex A was also found to transform to complex B, by rotation of the O_2 group. These results further strengthen the case for the stability of complex B.

All of the other complexes were unstable. An example of an instability that occurs is the sulfite ion dissociating into SO_2 and O^{2-} , with the SO_2 detaching from the Mn.

The structure of complex B in solution is shown in Fig. 7. In addition to the ligands, there are usually two water molecules strongly bound to the Mn; occasionally there was only one coordinating water in high acidity, and occasionally there were three strongly bound waters in neutral conditions. The Mn—O distances of complex B did not significantly vary with conditions,

and were 1.90 ± 0.02 Å, 1.98 ± 0.02 Å, and 2.05 ± 0.04 Å for the bonds with O atoms from O_2 , SO_3^{2-} , and H_2O , respectively. These bond lengths indicate that the Mn interacts most strongly with the O atoms from O_2 , and the least strongly with the O atoms from H_2O .

The results for the partial atomic charges for the atoms in complex B are shown in Fig. 8. Using the correlation in Eq. 6, the Mn formal charge was 3.5 ± 0.5 in neutral conditions, and 2.9 ± 0.3 in acidic conditions. Thus we find that the Mn is in the oxidation state of Mn(III) in acidic conditions, which is the condition in which the phenol degradation experiments were carried out.²³

To strengthen this conclusion, we examined the formal charges of the other atoms in complex B, to confirm that our analysis is self-consistent and that the sum of the formal charges in the complex balances with the formal charges of the ions in solution.

The formal charges of the atoms in the sulfite group in complex B are obtained by comparing the partial atomic charge of the S atom with that obtained in simulations of aqueous K_2SO_3 and K_2SO_4 , which dissociate in water into SO_3^{2-} and SO_4^{2-} , respectively. As shown in Fig. 9a, the partial atomic charge of S in complex B matches the result for aqueous SO_3^{2-} , and we thus conclude that the formal charges in the sulfite group of Complex B are the same as the standard values for an aqueous sulfite group: +4 for S and -2 for O.

The formal charges of the atoms in the O_2 group are obtained by comparing the O-O bond length in complex B with the bond length obtained in simulations of aqueous O_2 , as well as literature results for bond lengths in gas phase O_2 and for O_2^- and $O_2^{2^-}$ adsorbed on surfaces. As shown in Fig. 9b, the bond length for the O_2 group in complex B under neutral conditions falls between those for O_2^- and $O_2^{2^-}$, while the bond length in acidic conditions matches that for $O_2^{2^-}$. Thus the formal charge of these O atoms in neutral conditions is taken to be -0.75, and their formal charge in acidic conditions is taken to be -1.

The formal charge estimates for all atoms within complex B are shown in Fig. 10. We find internal consistency in that the sum of the formal charges for all ions in the system sums to zero, even though this condition was not enforced in the analysis—i.e., we independently determined the formal charge of the Mn ion, the formal charge of the sulfite group, and the formal charge of the O₂ group.

Overall, our simulations support the idea that Mn(III) is the oxidant in the $MnO_4^-/HSO_3^-/O_2$ catalysis system, and it can be stabilized by sulfite and dissolved O_2 ligands. Our simulations do not exclude the possible role of Mn(V) or Mn(VI) species, but we were not able to identify any Mn(V) or Mn(VI) complexes that were stable in water. We propose the following reaction mechanism through which $MnO_4^-/HSO_3^-/O_2$ oxidizes organic compounds. First, Mn(III) is generated by the reaction between MnO_4^- and HSO_3^- ,

$$2H^{+} + 2HSO_{3}^{-} + MnO_{4}^{-} \rightarrow Mn(III) + 2H_{2}O + 2SO_{4}^{2-}$$
 (7)

The Mn(III) is quickly complexed by O₂ and remaining HSO₃⁻ to form complex B,

$$Mn(III) + HSO_3^- + O_2 \rightarrow [Mn(III) - HSO_3^- - O_2]_B$$
(8)

which stabilizes the Mn(III) against disproportionation. Complex B then quickly oxidizes organic compounds, returning HSO₃⁻ and O₂ to solution,

$$[Mn(III) - HSO_3 - O_2]_B + organics \rightarrow products + Mn^{2+} + HSO_3 + O_2$$
 (9)

This mechanism can explain our previous findings that O_2 plays an important role in the MnO_4^- /HSO $_3^-$ system. Without O_2 , the reaction in Eq. 8 cannot occur and Mn(III) will undergo disproportionation rather than being stable. With O_2 , Mn(III) is stabilized by O_2 /HSO $_3^-$ in the form of complex B, which can act as an oxidant for organic contaminants (Eq. 9). After the oxidation reaction, HSO $_3^-$ and O_2 will be released (Eq. 9). Hence, we observe less consumption of HSO $_3^-$ and O_2 than when no organic contaminants are present. ²³

Our simulations also show that O_2 would be activated to $O_2^{2^-}$ under acidic conditions. This activated oxygen species may lead to the formation of OH radicals, which were recently discovered in $MnO_4^-/HSO_3^-/O_2$ systems and can serve as oxidants.⁵³

4. Conclusion

We examine charge distributions in aqueous manganese systems, and relate the charge distributions to Mn oxidation states. A nonlinear correlation between Mn partial atomic charge and oxidation state is found, with the dependence of partial atomic charge on oxidation state becoming weaker at higher oxidation states. This finding concurs with the feedback charge regulation process described previously³⁵ – as more charge is transferred to an atom, electron-electron repulsion causes the charge to spread out among other atoms, leading to a weakened dependence of partial atomic charge on oxidation state.

We use this correlation to address two open questions in water/wastewater treatment by Mn catalysts. First, our *ab initio* results for the average oxidation states of α , β and δ -MnO₂ are in excellent agreement with previous experiment results, ¹⁶ and support the idea that higher Mn(III) content leads to the faster organic contaminant degradation rates. Second, our simulations identify a ternary complex that stabilizes Mn(III) in the MnO₄⁻/HSO₃⁻/O₂ aqueous system, and may underlie the fast phenol degradation reaction found experimentally.²³

Acknowledgements

Our calculations were carried out using the high performance computing center at Case Western Reserve University. This work was supported by the National Science Foundation under Grant No. 1808406.

¹ R. Loos et al., "EU-wide survey of polar organic persistent pollutants in European river waters", Environ Pollut. 2009,157, 561-8.

- ² Kabir, E. R.; Rahman, M. S.; Rahman, I. A review on endocrine disruptors and their possible impacts on human health. Environ. Toxicol. Pharmacol. 2015, 40, 241–258
- ³ D. Voutsa, P. Hartmann, C. Schaffner, W. Geiger, "Benzotriazoles, Alkylphenols and Bisphenol A in Municipal Wastewaters and in the Glatt River, Switzerland", Environ Sci Pollut Res 13 (5) 333 341 (2006).
- ⁴ Xiong, W.; Sun, Y.; Ding, X.; Wang, M.; Zeng, Z. Selective pressure of antibiotics on ARGs and bacterial communities in manure-polluted freshwater-sediment microcosms. Front. Microbiol. 2015, 6, 194.
- ⁵ Zhang, H.; Huang, C.-H. Oxidative transformation of triclosan and chlorophene by manganese oxides. Environ. Sci. Technol. 2003, 37, 2421–2430
- ⁶ Lin, K.; Liu, W.; Gan, J. Oxidative removal of bisphenol A by manganese dioxide: efficacy, products, and pathways. Environ. Sci.Technol. 2009, 43, 3860–3864.
- ⁷ Zhang, H.; Taujale, S.; Huang, J.; Lee, G.-J. Effects of NOM onoxidative reactivity of manganese dioxide in binary oxide mixtures with goethite or hematite. Langmuir 2015, 31, 2790–2799
- ⁸ Nowack, B., Stone, A.T., 2002. Homogeneous and heterogeneous oxidation of nitrilotrismethylenephosphonic acid (NTMP) in the presence of manganese (II,III) and molecular oxygen. J. Phys. Chem. B 106, 6227-6233
- ⁹ Jiang, J., Pang, S.-Y., Ma, J., 2009. Oxidation of triclosan by permanganate (Mn(VII)): importance of ligands and in situ formed manganese oxides. Environ. Sci. Technol. 43, 8326-8331
- ¹⁰ Jiang, J., Pang, S.-Y., Ma, J., 2010. Role of ligands in permanganate oxidation of organics. Environ. Sci. Technol. 44, 4270-4275.
- ¹¹ Sun, B., Guan, X., Fang, J., Tratnyek, P.G., 2015. Activation of manganese oxidants with bisulfite for enhanced oxidation of organic contaminants: the involvement of Mn(III). Environ. Sci. Technol. 49, 12414-12421
- ¹² Gao, Y., Jiang, J., Zhou, Y., Pang, S.-Y., Ma, J., Jiang, C., Wang, Z., Wang, P.-X., Wang, L.-H., Li, J., 2017. Unrecognized role of bisulfite as Mn(III) stabilizing agent in activating permanganate (Mn(VII)) for enhanced degradation of organic contaminants. Chem. Eng. J. 327, 418-422.
- ¹³ Gao, Y., Jiang, J., Zhou, Y., Pang, S., technology, J.-C., 2018. Does soluble Mn (III) oxidant formed in situ account for enhanced transformation of triclosan by Mn (VII) in the presence of ligands? Environ. Sci. Technol. 52, 4785-4793.
- ¹⁴ Robinson, D. M.; Go, Y. B.; Mui, M.; Gardner, G.; Zhang, Z.; Mastrogiovanni, D.; Garfunkel, E.; Li, J.; Greenblatt, M.; Dismukes, G. C. Photochemical water oxidation by crystalline polymorphs of manganese oxides: structural requirements for catalysis. J. Am. Chem. Soc. 2013, 135 (9), 3494–3501.
- ¹⁵ Pokhrel, R.; Goetz, M. K.; Shaner, S. E.; Wu, X.; Stahl, S. S. The "best catalyst" for water oxidation depends on the oxidation method employed: a case study of manganese oxides. J. Am. Chem. Soc. 2015, 137 (26), 8384–8387.

¹⁶ J. Huang, S. Zhong, Y. Dai, C.-C. Liu, H. Zhang, Effect of MnO₂ phase structure on the oxidative reactivity toward bisphenol A degradation, Environ. Sci. Technol. 52 (2018) 11309–11318.

¹⁷ Cheng, F.; Zhang, T.; Zhang, Y.; Du, J.; Han, X.; Chen, J., "Enhancing Electrocatalytic Oxygen Reduction on MnO2 with Vacancies" Angew. Chem., Int. Ed. 2013, 52, 2474-2477.

- ¹⁸ D. A. Tompsett, S. C. Parker, M. S. Islam, "Rutile (b-)MnO2 surfaces and vacancy formation for high electrochemical and catalytic performance", J. Am. Chem. Soc. 136, 1418-1426 (2014). ¹⁹ H. Peng et al., "Redox properties of birnessite from a defect perspective", Proc. Natl. Acad. Sci. 114, 9523-9528 (2017).
- ²⁰ R. H. Waldemer and P. G. Tratnyek, "Kinetics of contaminant degradation by permanganate", Environ. Scie. Technol. 40, 1055-1061 (2006).
- ²¹ O. W. Duckworth and G. Sposito, "Diserophore-Manganese(III) interactions. I. Air-oxidation of manganese(II) promoted by desfererrioxamine B", Environ. Sci. Technol. 39, 6037-6044 (2005).
- ²² A. S. Madison B. M. Tebo, A. Mucci B. Sundby, G. W. Luther III, "Abundant porewater Mn(III) is a major component of the sedimentary redox system", Science 341, 875 (2013).
- ²³ S. Zhong and H. Zhang, "New insight into the reactivity of Mn(III) in bisulfite/permanganate for organic compounds oxidation: the catalytic role of bisulfite and oxygen", Water Research, 148, 198-207 (2019).
- ²⁴ Gao, Y.; Zhou, Y.; Pang, S.-Y.; Jiang, J.; Yang, Z.; Shen, Y.; Wang, Z.; Wang, P.-X.; Wang, L.-H., New Insights into the Combination of Permanganate and Bisulfite as a Novel Advanced Oxidation Process: Importance of High Valent Manganese-Oxo Species and Sulfate Radical. Environmental Science & Technology 2019.
- ²⁵ Chen, J.; Rao, D.; Dong, H.; Sun, B.; Shao, B.; Cao, G.; Guan, X., The role of active manganese species and free radicals in permanganate/bisulfite process. Journal of Hazardous Materials 2020, 388, 121735.
- ²⁶ A. Walsh, A. A. Sokol, J. Buckeridge, D. O. Scanlon, C. R. A. Catlow, "Oxidation states and iconicity", Nature Materials 17, 958 (2018).
- ²⁷ P. Karen, "Oxidation state, a long-standing issue!", Angew. Chem. Intl. Ed. 54, 4716-4726 (2015).
- ²⁸ R. Resta, "Charge states in transition", Nature 435, 735 (2008).
- ²⁹ M. Jansen, U. Wedig, "A piece of the picture misunderstanding of chemical concepts", Angew. CHem. Int. Ed. 47, 10026-10029 (2008).
- ³⁰ G. Aullon, S. Alvarez, "Oxidation states, atomic charges and orbital populations in transition metal complexes", Theor. Chem. Acc. 123, 67-73 (2009).
- ³¹ B. Wang, S. L. Li, D. Truhlar, "Modeling the partial atomic charges in inorganometallic molecules and solids and charge redistribution in lithium-ion cathodes", J. Chem. Theory Comput. 10, 5640-5650 (2014).
- ³² P. T. Wolczanski, "Flipping the oxidation state formalism: charge distribution in organometallic complexes as reported by carbon monoxide, Organometallics 36, 622-631 (2017).
- ³³ A. Walsh, A. A. Sokol, J. Buckeridge, D. O. Scanlon, C. R. A. Catlow, "Electron counting in solids: oxidation states, partial charges, and ionicity", J. Phys. Chem. Lett. 8, 2074-2075 (2017). ³⁴ D. Koch, S. Manzhos, "On the Charge State of Titanium in Titanium Dioxide", J. Phys. Chem. Lett. 8, 1593–1598 (2017).

³⁵ H. Raebiger, S. Lany, A. Zunger, "Charge self-regulation upon changing the oxidation state of transition metals in insulators", Nature 435, 763-766 (2008).

- ³⁶ G. A. E. Oxford and A. M. Chaka, "First-principles calculations of clean, oxidized and reduced □-MnO2 surfaces, J. Phys. Chem. C 115, 16992-17008 (2011).
- 37 L.-C. Hsu, M.-K. Tsai, Y.-H. Lu, H.-T. Chen, "Computational investigation of CO adsorption and oxidation on Mn/CeO₂(111) surface" J. Phys. Chem. C 117, 433-441 (2013).
- ³⁸ K. Alexopoulos, Y. Wang, D. G. Vlachos, "First-principles kinetic and spectroscopic insights into single-atom catalysis", ACS Catal. 9, 5002-5010 (2019).
- ³⁹ S. K. Iyemperumal and N. A. Deskins, "Activation of CO2 by supported Cu clusters", Phys. Chem. Chem. Phys. 19, 28788-28807 (2017).
- ⁴⁰ J. M. Soler, E. Artacho, J. D. Gale, A. García, J. Junquera, P. Ordejón, and D. Sánchez-Portal, "The SIESTA method for ab initio order-N materials simulation", J. Phys. Condens. Matter, 14, 2745-2780 (2002).
- ⁴¹ D. S. Sholl and J. A. Steckel, Density Functional Theory: A Practical Introduction, John Wiley & Sons, Inc., 2009
- ⁴² H. J. C. Berendsen, D. van der Spoel, R. van Drunen, "GROMACS: A message-passing parallel molecular dynamics implementation", Comput. Phys. Commun. 91, 43–56 (1995).
- ⁴³ J. P. Perdew, K. Burke, and M. Ernzerhof, "Generalized gradient approximation made simple", Phys. Rev. Lett., 77, 3865-3868 (1996).
- ⁴⁴ N. Troullier and J. L. Martins, "Efficient pseudopotentials for plane-wave calculations", Phys. Rev. B Condens. Matter, 43, 1993-2006 (1991)
- ⁴⁵ R. Bader, Atoms in Molecules: A Quantum Theory, Oxford University Press, 1994.
- ⁴⁶ G. Henkelman, A. Arnaldsson, and H. Jónsson, "A fast and robust algorithm for Bader decomposition of charge density", Comput. Mater. Sci., 36, 354-360 (2006).
- ⁴⁷ E. Artacho, J. M. Cela, J. D. Gale, A. García, J. Junquera, R. M. Martin, P. Ordejón, N. R. Papior, D. Sánchez-Portal, and J. M. Soler, "SIESTA 4.1-b4 user's guide" (2018).
- ⁴⁸ D. A. Tompsett, S. C. Parker and M. S. Islam, "Surface properties of □-MnO₂: relevance to catalytic and supercapacitor behaviour", J. Mater. Chem. A 2, 15509 (2014).
- 49 G. A. E. Oxford and A. M. Chaka, "Structure and Stability of hydrated \Box -MnO₂ surfaces", J. Phys. Chem. C 116, 11589-11605 (2012).
- ⁵⁰ Z. Ding, A. Selloni, "Hydration structure of flat and stepped MgO surfaces", J. Chem. Phys. 154 114708 (2021)
- ⁵¹ R. R. Rao et al., "Surface Orientation Dependent Water Dissociation on Rutile Ruthenium Dioxide", J. Phys. Chem. C. 122, 17802-17811 (2018).
- ⁵² U. Aschauer, J. Chen, and A. Selloni, "Peroxide and superoxide states of adsorbed O₂ on anatase TiO₂ (101) with subsurface defects", Phys. Chem. Chem. Phys., 12, 12956-12960 (2010).
- 53 Shi, Z.; Jin, C.; Zhang, J.; Zhu, L., Insight into mechanism of arsanilic acid degradation in permanganate-sulfite system: Role of reactive species. Chemical Engineering Journal 2019, 359, 1463-1471.

Table 1. Inputs and results for simulations that were used to develop the correlation between Mn oxidation state and partial atomic charge.

Input		Results				
Ion complex	Additional atoms	Ions in solution	Z_{Mn-X}	Z_{Mn}	Q _{Mn}	
MnO_4 $Z_X = -8$	6 K	6 K ⁺	-6.00	+2.00	+1.36	
	5 K	5 K ⁺	-5.00	+3.00	+1.65	
	4 K	4 K ⁺	-4.00	+4.00	+1.72	
	3 K	3 K ⁺	-3.00	+5.00	+1.81	
	2 K	2 K ⁺	-2.00	+6.00	+1.86	
	1 K	1 K ⁺	-1.00	+7.00	+1.89	
	1 K	1 K ⁺	-1.00	+2.00	+1.40	
$Mn-NTA$ $Z_X = -3$			0.00	+3.00	+1.69	
	1 Cl	1 Cl ⁻	+0.99	+3.99	+1.79	
	2 Cl	2 C1 ⁻	+1.92	+4.92	+1.86	
	3 Cl	2 Cl ⁻ , 1 H ₃ O ⁺	+0.95	+3.95	+1.79	
Mn-EDTA	2 K	2 K ⁺	-2.00	+2.00	+1.38	
	1 K	1 K ⁺	-1.00	+3.00	+1.65	
			0.00	+4.00	+1.72	
	1 Cl	1 H ₃ O ⁺	-1.00	+3.00	+1.64	
$Z_X = -4$	1 Cl	1 Cl ⁻	+0.70	+4.70	+1.76	
	2 Cl	1 Cl ⁻ , 1 H ₃ O ⁺	-0.03	+3.97	+1.74	
	3 Cl	1 Cl ⁻	+0.81	+4.81	+1.75	
	2 K	2 K ⁺	-2.00	+2.00	+1.37	
Mn-PP	1 K	1 K ⁺	-1.00	+3.00	+1.70	
			0.00	+4.00	+1.69	
$Z_X = -4$	1 Cl	1 Cl ⁻	+0.98	+4.98	+1.85	
	2 Cl	2 C1 ⁻	+1.35	+5.35	+1.88	
	3 Cl	2 Cl ⁻ , 1 H ₃ O ⁺	+0.90	+4.90	+1.87	
Mn ion $Z_X = 0$	2 Cl	2 Cl ⁻	+1.97	+1.97	+1.36	
	3 Cl	3 Cl ⁻	+2.66	+2.66	+1.53	
	4 Cl	4 Cl ⁻	+3.27	+3.27	+1.64	
	5 Cl	5 Cl ⁻	+4.48	+4.48	+1.85	
	5 Cl	3 Cl ⁻	+2.87	+2.87	+1.70	
	6 Cl	6 Cl ⁻	+4.63	+4.63	+1.81	
	7 Cl	7 Cl ⁻	+5.65	+5.65	+1.86	

Table 2. Results for partial atomic charges and oxidation states of Mn atoms in the nanoscale MnO_2 polymorphs. Each row represents a group of Mn atoms that are equivalent by symmetry. Results shown are the averages for the symmetrically equivalent atoms, and the uncertainty shown is the standard error (an uncertainty estimate is not given when there is only one atom in the group). The oxidation state is obtained from the partial atomic charge using Eq. 6.

	Coordination number in	Number of equivalent	Partial atomic charge (e)	Oxidation state
	crystallite	atoms		
α-MnO ₂	3	4	1.79 ± 0.02	4.4 ± 0.3
	4	4	1.705 ± 0.007	3.46 ± 0.06
	5	4	1.78 ± 0.02	4.2 ± 0.2
	6	4	1.73 ± 0.03	3.7 ± 0.3
β-MnO ₂	2	2	1.82 ± 0.01	4.9 ± 0.3
	3	2	1.73 ± 0.03	3.7 ± 0.2
	4	2	1.84 ± 0.01	5.4 ± 0.4
	4	1	1.67	3.2
	5	2	1.71 ± 0.01	3.51 ± 0.09
	6	1	1.73	3.7
δ-MnO ₂	4	2	1.79 ± 0.07	4.7 ± 1.1
	4	2	1.76 ± 0.03	4.0 ± 0.3
	5	4	1.67 ± 0.03	3.3 ± 0.2
	6	1	1.62	2.9

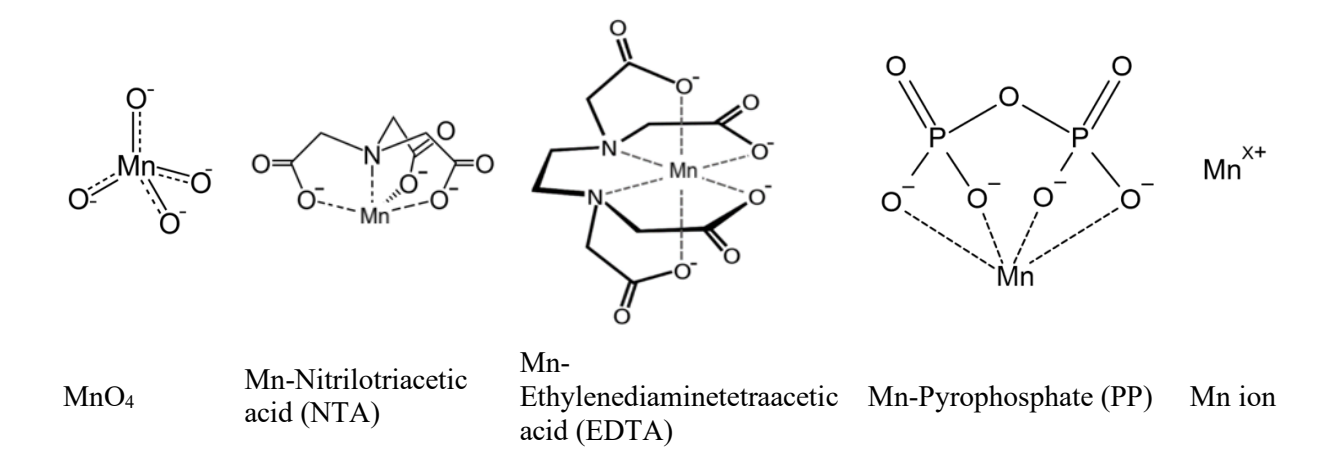


Figure 1. Mn ion complexes used to generate the correlation between Mn partial atomic charge and oxidation state.

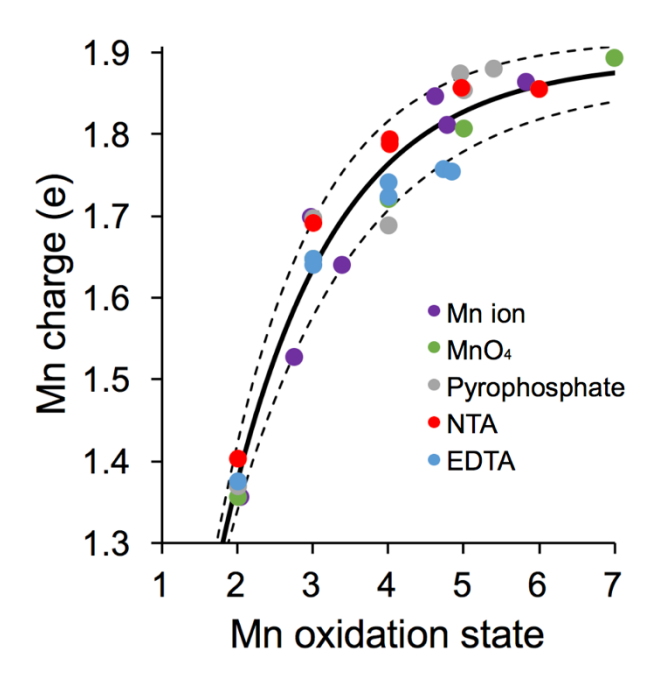


Figure 2. Mn partial atomic charge as a function of Mn oxidation state, for the systems listed in Table 1. The Mn oxidation state was calculated with Eq. 5. The fit (solid line) was obtained with least-squares regression, and error bounds (dashed lines) are obtained with parameters that differ from the best-fit values by plus and minus one standard error.

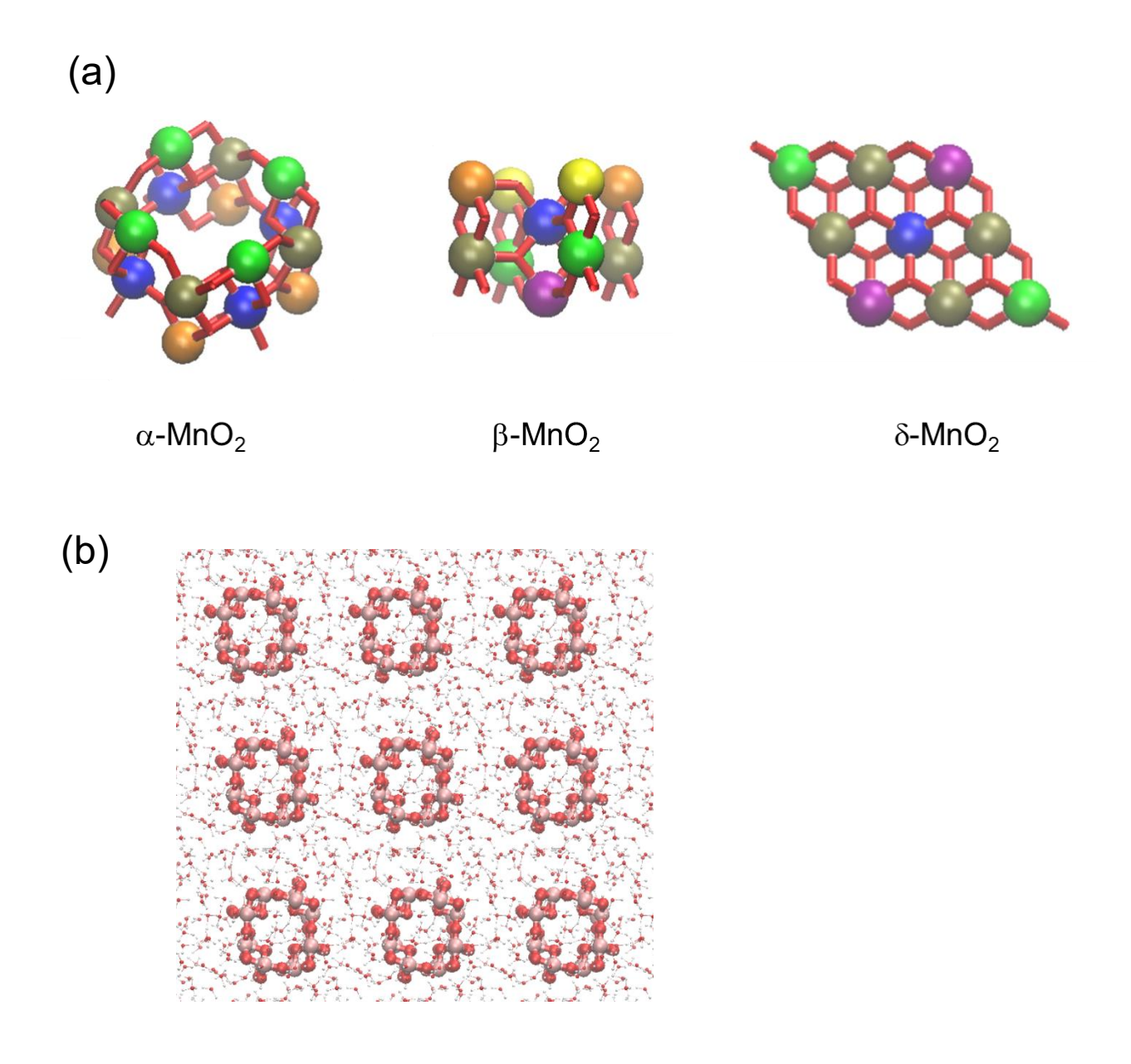
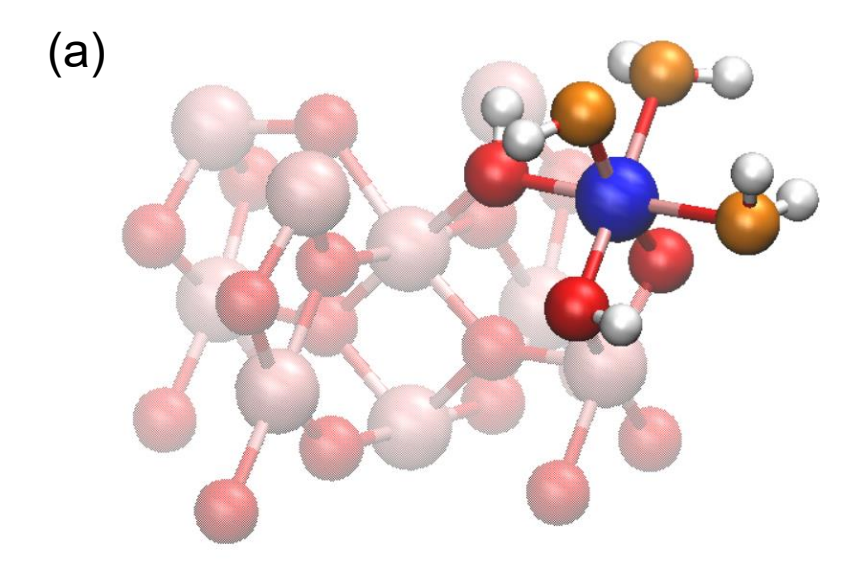


Figure 3: (a) MnO₂ structures examined in this study. Oxygen atoms are at the vertices and ends of the red bars. Mn atoms are shown as spheres, where spheres of the same color are positions that are equivalent by symmetry. The color of an Mn atom identifies the number of oxygen atoms coordinated to it: yellow=2; orange=3; green and purple=4; tan=5; blue=6. (b) The system studied in the α -MnO₂ simulations, which includes the polymorph (larger atoms) and water (smaller atoms); periodic boundary conditions are used, and the simulation cell corresponds to the central part of this figure.



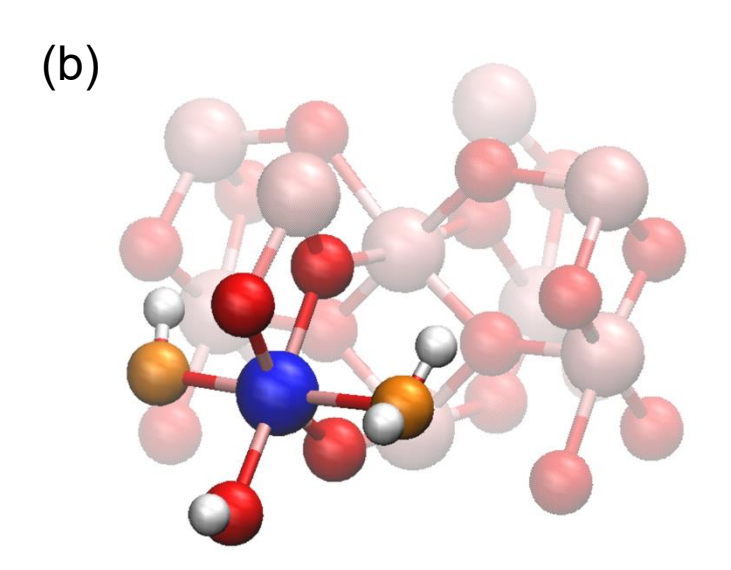


Figure 4: Snapshots from the β-MnO₂ simulation highlighting the interaction of two Mn atoms with water. (a) The featured Mn atom (blue) is bonded to three crystal O atoms (red), two of which gained H^+ ions and became OH^- groups. The featured Mn atom is also bonded to three O atoms from water (orange), one of which lost an H^+ ion and thus became an OH^- group. (b) The featured Mn atom (blue) is bonded to four crystal O atoms (red), one of which gained an H^+ ion and became an OH^- group. The featured Mn atom is also bonded to two O atoms from water (orange), one of which lost an H^+ ion and thus became an OH^- group.

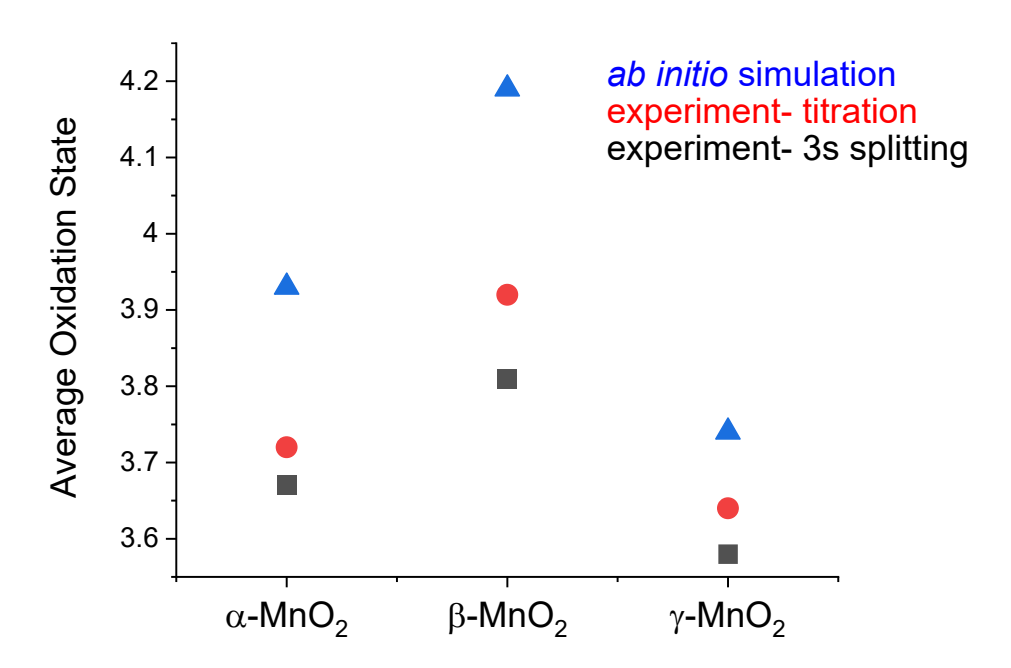


Figure 5: Average oxidation states of Mn atoms in MnO₂ polymorphs. The experimental results are from reference 16.

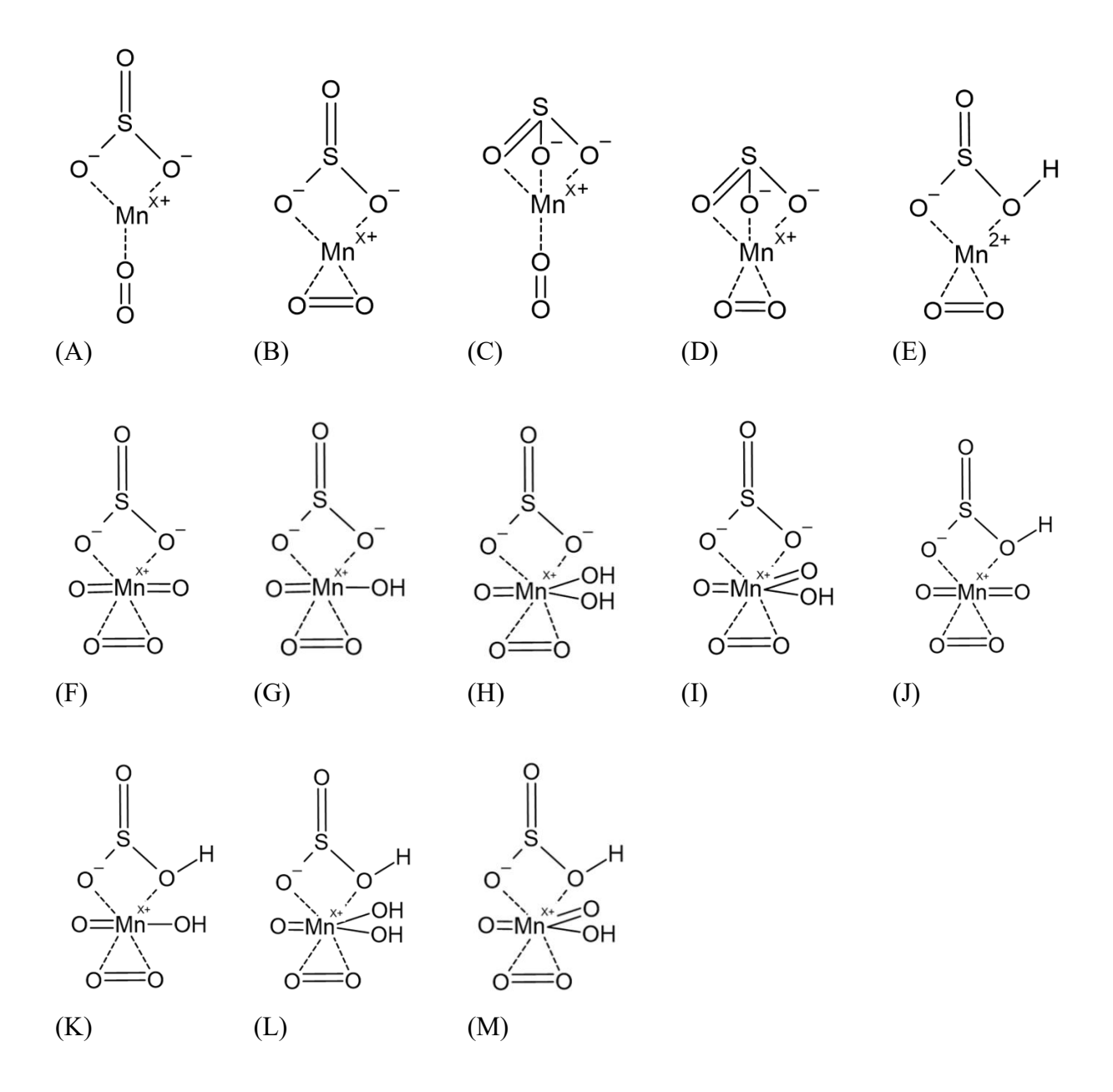


Figure 6. Complexes examined as possible catalytic species in the $MnO_4^-/HSO_3^-/O_2$ system. Complex B was the only structure that remained stable for the simulation duration.

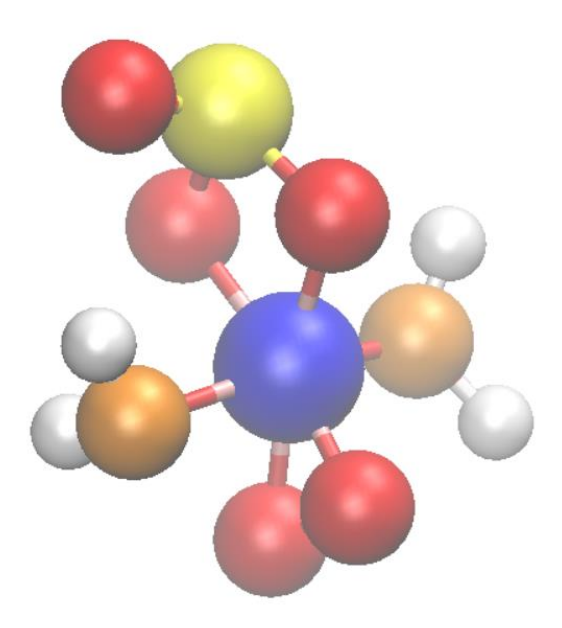


Figure 7. Snapshot from the simulation of complex B, including the interaction of the Mn atom with water. The Mn atom (blue) is bonded to four O atoms from the complex (red), and also to two O atoms from water (orange). The SO_3^{2-} group is above the Mn (S atom is yellow), and the O_2 group is below the Mn.

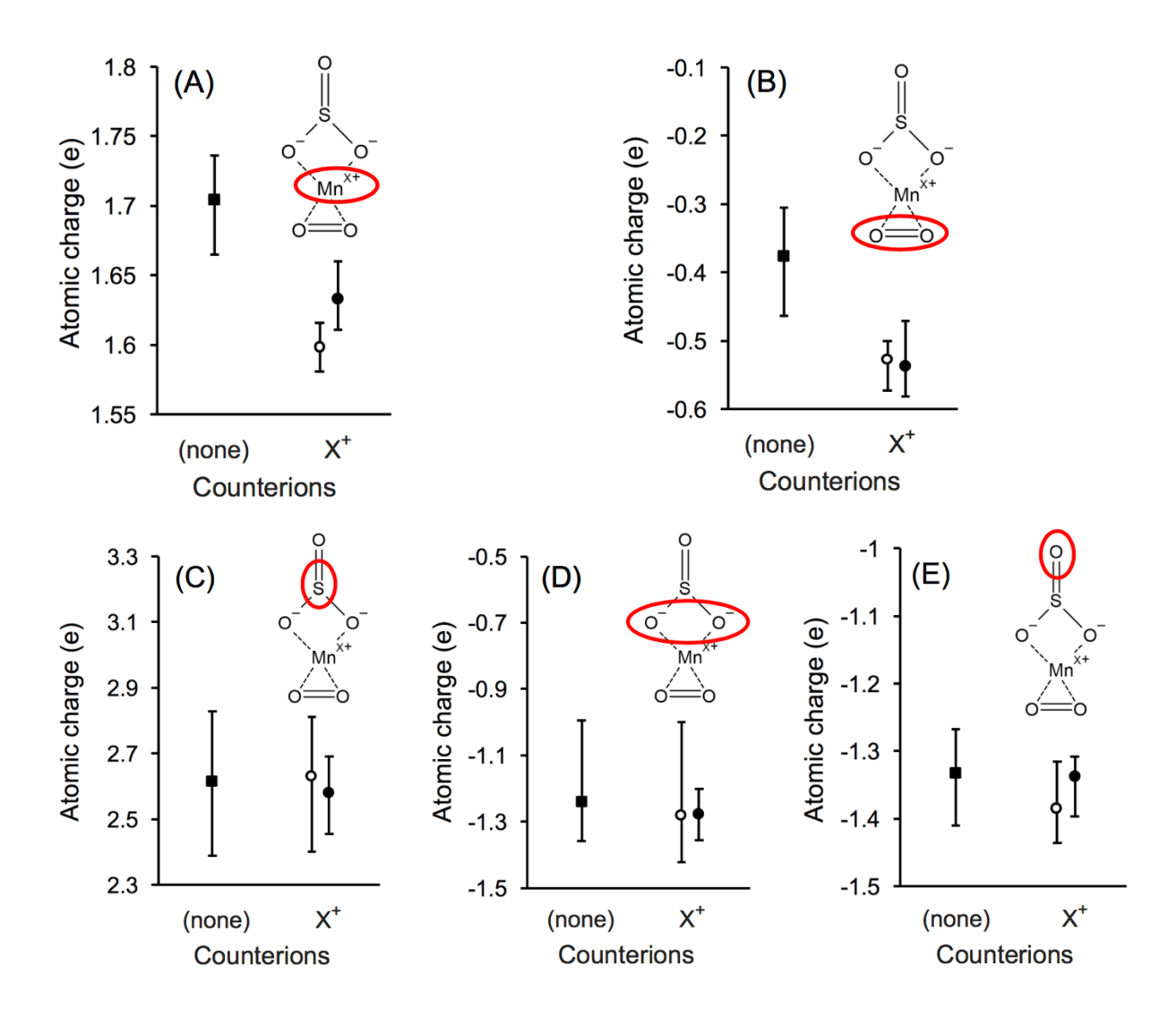


Figure 8. Partial atomic charges for atoms within complex B: (A) Mn atom, (B) O atoms from the O_2 group, (C) S atom, (D) O atoms from the sulfite group that are coordinated to Mn, and (E) O atom from the sulfite group that is not coordinated to Mn. For the results with one counterion, open circles represent simulations with H^+ and closed circles represent simulations with K^+ . Error bars denote the maximal and minimal values observed in the simulation.

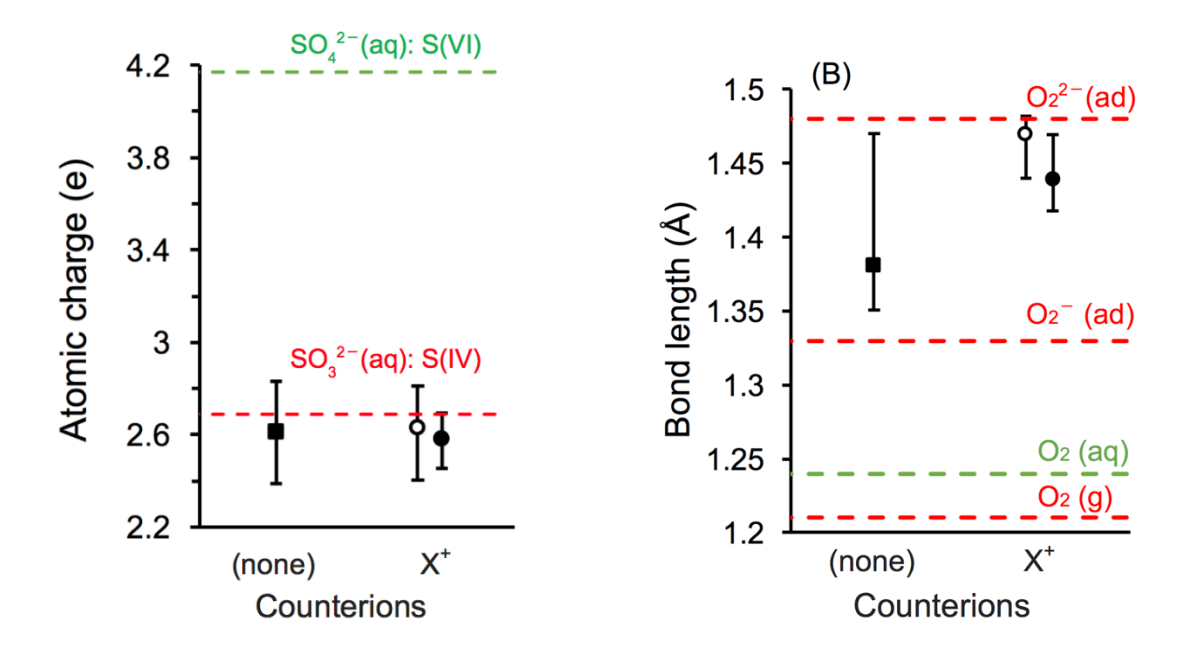


Figure 9. (A) Atomic charges of the S atom in complex B, compared with results of simulations of aqueous K_2SO_3 and K_2SO_4 . (B) Bond length of the O_2 group in complex B, in comparison to simulation results for the bond length in aqueous O_2 , and literature results⁵² for the bond lengths in gas phase O_2 and adsorbed O_2^- and O_2^{2-} . For the results with one counterion, open circles represent simulations with H^+ and closed circles represent simulations with K^+ . Error bars denote the maximal and minimal values observed in the simulation.

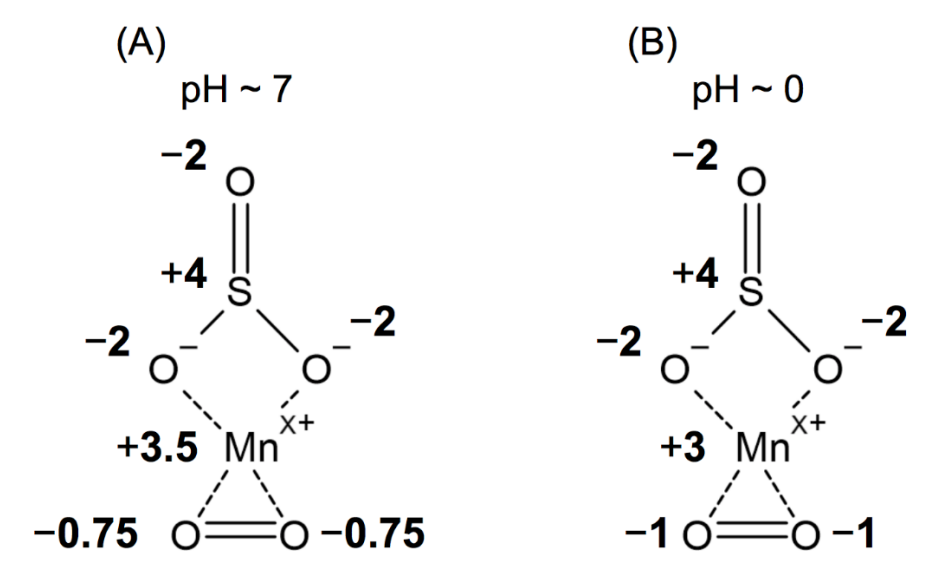


Figure 10. Proposed formal charges for atoms in complex B under (A) neutral and (B) acidic conditions, based on the correlation between Mn partial atomic charge and oxidation state (Fig. 2), comparison of S partial atomic charge to that for known aqueous ions (Fig. 7a), and the relationship between O₂ bond length and formal charge (Fig. 7b).